Princeton Plasma Physics Laboratory

PPPL- 4834

PPPL- 4834

Formation and Sustainment of ITPs in ITER with the Baseline Heating Mix

Francesca M. Poli and Charles Kessel

November, 2012

Prepared for the U.S. Department of Energy under Contract DE-AC02-09CH11466.

Princeton Plasma Physics Laboratory
Report Disclaimers

Full Legal Disclaimer

Trademark Disclaimer

PPPL Report Availability

Princeton Plasma Physics Laboratory:

http://www.pppl.gov/techreports.cfm

Office of Scientific and Technical Information (OSTI):

http://www.osti.gov/bridge

Related Links:

U.S. Department of Energy

Office of Scientific and Technical Information

Fusion Links

Formation and sustainment of ITBs in ITER with the baseline heating mix

Francesca M. Poli[1, a)] and Charles E. Kessel[1]

Princeton Plasma Physics laboratory, Princeton, NJ, 08543

(Dated: 30 November 2012)

Plasmas with internal transport barriers (ITBs) are a potential and attractive route to steady-state operation in ITER. These plasmas exhibit radially localized regions of improved confinement with steep pressure gradients in the plasma core, which drive large bootstrap current and generate hollow current profiles and negative shear. This work examines the formation and sustainment of ITBs in ITER with electron cyclotron heating and current drive. It is shown that, with a trade-off of the power delivered to the equatorial and to the upper launcher, the sustainment of steady-state ITBs can be demonstrated in ITER with the baseline heating configuration.

PACS numbers: 52.25.Xz, 52.55.Fa

[a)] fpoli@pppl.gov

I. INTRODUCTION

Plasmas with internal transport barriers (ITBs) are a potential and attractive route to steady-state operation in ITER. These plasmas exhibit radially localized regions of improved confinement with steep pressure gradients in the plasma core, which drive large bootstrap current, which in turn generates hollow current profiles and hence negative magnetic shear in the core. Extensive reviews of the physics and of the main characteristics of ITBs observed in present day experiments are provided in the papers by Connor *et al*[1], Litaudon[2], Staebler[3] and Wolf[4].

In order to achieve fusion gain of $Q \simeq 5$ at a plasma current of 9MA, steady state scenarios on ITER should get a 60% improvement over the H-mode confinement time, *i.e.* $H_{98} \geq 1.6$, which will likely be obtained only with internal transport barriers.

Theories of ITB formation often rely on turbulence suppression mechanisms by sheared $\mathbf{E} \times \mathbf{B}$ flow[1,3,5]. However, the flow shear stabilization from toroidal rotation is expected to be low in ITER and the same mechanisms that are at play in present-day experiments may not work in ITER.

Since transport models used for H-mode plasmas (like the baseline and the hybrid scenarios) that are dominated by $\mathbf{E} \times \mathbf{B}$ rotational shear stabilization have deficiencies when applied to reversed shear plasmas and high pressures, simulations of steady state scenarios with ITBs often prescribe the thermal diffusivity profile with an analytic form[6–8] or use semi-empirical methods[9,10]. The first approach is suitable for steady state analysis and parameter scan studies, since it does not contain a trigger for ITBs, while the second approach is also suitable for ITB formation studies. With a hypothesis made on the confinement gain (usually $H_{98} \sim 1.6$), the results obtained with both approaches set reasonable boundaries to the plasma performance and to the range of parameters expected.

With constraints on the transport (an analytic thermal diffusivity profile and $H_{98} \sim 1.6$) and assuming sustained ITBs in the flattop phase, it was shown in a previous work[8] that the ITER baseline heating mix (33MW of NB, 20MW of IC and 20MW of EC) can sustain up to 7.4 MA of non-inductive current, it achieves fusion gain $Q \sim 2.2$ and is ideal MHD stable around the operational point. In this work, we use the Current Diffusive Ballooning Mode (CDBM) transport model[11–13] to examine the formation of ITBs in L-mode and their sustainment in the flattop phase. It will be shown that by trading-off the power delivered

to the equatorial and to the upper launcher, ITBs can be triggered in L-mode in reverse shear plasmas and sustained in the flattop for a time sufficiently long to avoid coil currents to reach their limits. The plasma current exceeds the total non-inductive current leading to some level of Volt-second consumption.

Section II introduces the simulation codes used for calculation of the scenario and for the transport analysis and the geometrical settings of the electron cyclotron upper launcher. The effect of the launching configuration on the formation and sustainment of ITBs is discussed respectively in Sec.III A and Sec.III B. The conditions for sustainment of steady-state barriers are discussed in Sec.IV where it is presented a scenario that attempts at maximizing the non-inductive driven current predicted by the CDBM transport model.

II. SCENARIO DEVELOPMENT

All simulations begin with a large bore 500 kA plasma, which is grown to full size and shape by ~ 14 s, at which time the X-point forms and the plasma is diverted, at $I_P = 3\,\mathrm{MA}$. The target plasma has $R = 6.2$ m, $a = 2.0$ m, elongation $\kappa \sim 1.8$ and triangularity $\delta \sim 0.45$[7,8].

Full plasma discharges are simulated with the Tokamak Simulation Code[14] (TSC), a predictive, free boundary transport evolution code. The free-boundary plasma equilibrium and field evolution equations are solved on a two-dimensional Cartesian grid, while the surface-averaged transport equations for the pressure and densities are solved in magnetic flux coordinates.

Neoclassical-resistivity, bootstrap-current, auxiliary-heating, current-drive, alpha-heating and radiation are all included. TSC uses a 2D representation of the central solenoid, of the poloidal field coils and of the surrounding conducting structures. Feedback systems for plasma position, shape and current are also included. TSC is used to establish the scenario in terms of all parameters as a function of time, targeting the desired properties of the scenario and attempting to remain within all limits.

TSC can be viewed as providing experimental-like conditions: the plasma boundary, the density, temperature and impurities profiles, the total plasma current. These are input to TRANSP[15], a prescribed boundary transport evolution code, which calculates the profiles of heating deposition and current that are then given back to TSC for re-calculation of the

scenario.

A. Heating and Current Drive Sources

The ITER steady state scenario is significantly dependent on the heating and current drive sources, since the current profiles, in combination with the bootstrap current, determine the safety factor profile. The external power heating sources considered herein are 33 MW of neutral beam (NB), 20 MW of ion cyclotron (IC) and 20 MW of electron cyclotron (EC), the so-called 'day one heating mix'. Each source has defined parameters such as frequency, particle energy, spectra, and steering angle.

Ion cyclotron model. The ICRF source model is the TORIC full wave[16] with a Fokker Planck treatment of the resonant species and equivalent Maxwellians for other fast species (neutral beam ion and alpha particles). The ICRH uses Helium-3 ion minority heating at a concentration of 2% of the electron density and a frequency of 48 MHz for on-axis deposition and to accommodate the strong magnetic axis shift.

Neutral beam model. The NB source model is the NUBEAM orbit following Monte Carlo[17,18]. The NB has 1 MeV particle energy, with the capability to steer from on-axis to off-axis. Unless otherwise specified, the simulations presented herein use one beam on-axis and one beam off-axis, providing deposition profiles peaked at normalized radius $\rho \sim 0.3$ and up to $\sim 3\,\mathrm{MA}$ of non-inductive current for 33 MW of injected power.

Electron cyclotron model. The electron cyclotron heating and current drive are calculated with TORAY, a ray-tracing 1D Fokker Planck code[19], which includes relativistic effects, electron-ion collisions and trapped particle effects.

The ITER electron cyclotron system will deliver 20MW for heating and current drive, which can be diverted to either an equatorial launcher (EL) or an upper launcher (UL) by means of a switch in the transmission line[20]. The UL provides highly localized, off-axis power deposition in the range of $\rho = [0.45, 0.8]$ for control of MHD instabilities like Neoclassical Tearing Modes, distributing the power in two rows: an upper (USM) and a lower (LSM) steering mirror[20,21]. The current drive efficiency is about 25% of the efficiency of the EL, which in these simulations is steered to deposit at $\rho \simeq 0.40$.

B. Transport models

Particle transport models are not used in this work, instead the electron density profiles are prescribed, as the superposition of a broad profile for the H-mode and a peaked profile that imitates the ITB. The Helium concentration is determined by an input $\tau^*_{\rm He}/\tau_{\rm E} = 5$ and includes the buildup to burn conditions. The Hydrogen (DT) fuel density is determined from quasi-neutrality assuming equal amounts of D and T. The impurity density profiles are assumed to be the same as the electron density, with their fractions prescribed as a function of time. A concentration of 2% Beryllium and 0.4% of Argon provides about 20MW of core radiated power (bremsstrahlung, cyclotron and line) and brings the conducted power to the divertor to $\sim$ 80MW.

The thermal diffusivity profile is computed using either a modified Coppi-Tang model[6] or the CDBM model[12], which has been recently implemented in TSC.

Coppi-Tang transport model. A semi-empirical approach is adopted to produce an ITB in the electron and ion temperature through a modified thermal diffusivity profile: a combination of an L-mode Coppi-Tang model for the interior region[22,23] and two terms to model, respectively, the ITB foot and the pedestal[6]. Inside the barrier, $\rho < \rho_{\rm b}$, the diffusivity is calculated as $[1 + C_1(1 - \rho/\rho_{\rm b})^2]$. The parameter C_1 modifies the thermal diffusivity on axis responding to the magnetic shear: higher values of C_1 are associated with stronger reverse shear and temperature profiles more flat in the core, while lower values are associated with weak reverse shear profiles and parabolic profiles. We approximate $\chi(0)/\chi_{\rm min} = q_0/q_{\rm min}$ and adjust $\rho_{\rm b}$ according to the safety factor profile, based on experimental evidence that - in reverse shear plasmas - ITBs are locked to the radius of the minimum safety factor. The thermal diffusivity is dropped at the edge to reproduce the desired pedestal temperature, with pedestal width and height being set by the EPED1 peeling-ballooning ideal MHD stability model[24]. The reshaped profile is then scaled to match $H_{98} \sim 1.6$, while maintaining $T_{\rm ped}$ in the correct range. The results obtained with the Coppi-Tang model on the baseline heating mix scenario are reported in the first column of Table I and they will compared to the CDBM model in Sec.III B.

CDBM transport model. This model is based on the theory of self-sustained turbulence due to current diffusivity driven modes[11]. The thermal diffusivities are computed as the

sum of a neoclassical term and a turbulence term $\chi_{\rm T}$[12,13]:

$$\chi_{\rm T} = 12\ F(s,\hat{\alpha}) F_\kappa F_{\rm E} \alpha^{3/2} \frac{c^2}{\omega_{\rm pe}^2} \frac{v_{\rm A}}{qR} \tag{1}$$

where c is the speed of light, $\omega_{\rm pe}$ the electron plasma frequency, $v_{\rm A}$ the Alfvén velocity and $\alpha \equiv -q^2 R(d\beta/dr)$ the normalized pressure gradient. The same $\chi_{\rm T}$ holds both for ions and electrons, since the CDBM model does not distinguish between species. The factor $F(s,\hat{\alpha})$ represents the reduction in the thermal diffusivity due to weak or negative magnetic shear and large Shafranov shift[12]. It is a function of the magnetic shear $s \equiv rq^{-1}(dq/dr)$ and of the normalized MHD pressure gradient $\hat{\alpha}$, which includes the fast ion contribution. Plasma shape effects are included in the factor F_κ[25]. The term $F_{\rm E} = [1 + \omega_{\rm E}^2/\gamma^2]^{-1}$ models the $\mathbf{E}\times\mathbf{B}$ flow shear turbulence stabilization, where γ is the growth rate of the most unstable mode[11], $\gamma^{-1} = (6s/\alpha)^{1/2}(qR/v_A)$. The shearing frequency $\omega_{\rm E}$ is defined according to Hahm and Burrell[26], assuming isotropic turbulence in the plane perpendicular to the magnetic field, and the radial electric field is derived from the radial ion force balance equation:

$$E_{\rm r} = \frac{1}{Z_{\rm i} e n_{\rm i}} \frac{\partial p_{\rm i}}{\partial r} + B_\theta v_{\phi,{\rm i}} - B_\phi v_{\theta,{\rm i}} \tag{2}$$

The ion poloidal velocities are computed with the NCLASS transport model[27] in TRANSP, while the toroidal velocity is calculated assuming $\chi_\phi = \chi_{\rm i}$. A value of $\chi_\phi = 0.3\chi_{\rm i}$ results in a correction of 4% in the central temperature and less than 1% in the non-inductive current in the flat-top phase, indicating that the plasma toroidal rotation is a small contribution.

The scaling parameter in front of $\chi_{\rm T}$ provides the correction between the CDBM confinement time and the ITER τ_{89} in the absence of the stabilizing terms $F(s,\hat{\alpha})$ and F_E[12]. The CDBM is a core transport model and, as such, is not valid in the pedestal region. Thus, we use the CDBM model inside $\rho = 0.75$, the Coppi-Tang model (previously discussed) outside this radius and an hyperbolic function to match the two.

III. FORMATION AND SUSTAINMENT OF AN ITB

This section discusses the conditions for formation of ITBs in the ramp-up phase and for their sustainment in the flat-top. We consider two cases, with same total delivered power, but different distribution between the equatorial and the upper launcher. The first configuration has 13.4MW of EC on the EL and 6.7MW on the UL (hereafter configuration

#1), the second has all the available power delivered to the UL (configuration #2). The same heating configuration is maintained throughout the whole plasma discharge and the EC deposition radius of the upper launcher for this study is chosen at $\rho \simeq 0.6$, where the UL drives the maximum current (as it will be discussed in Sec.IV). It will be shown that configurations with a larger fraction of EC power delivered to the UL sustain larger bootstrap fraction in the flattop phase. However, the combination of external driven current and bootstrap current do not maintain reverse shear in the core and safety factor minimum in the outer mid-radius, causing the ITBs to diffuse inward.

A. Formation of ITBs in the ramp-up phase

Figure 1 (left column) shows the profiles of temperature, safety factor and EC heating for the two configurations, calculated at $t = 55$s. At the low L-mode densities in the early ramp-up phase, the central electron heating provided by the equatorial launcher forms reverse shear profiles that trigger ITBs in the electron channel. With all the EC power delivered to the upper launcher, configuration #2 has magnetic shear positive in the core in L-mode. However, the localized EC heating at $\rho \simeq 0.6$ favors the formation of a minimum in the q-profile with weakly reversed magnetic shear. The CDBM model responds to this profile variation off-axis, causing a decrease in the transport and the steepening of the ion and electron temperature profiles at $\rho \simeq 0.6$.

Figure 2 shows the evolution of the total power inside the electron (a) and the ion (b) barrier, the minimum value of the magnetic shear (c), which is calculated over the outer mid-radius in the case of configuration #2, the ITB foot location (d), the maximum inverse electron temperature gradient scale length $L_{\mathrm{T_e}}^{-1}$ (e), and the term $f(s, \hat{\alpha})$ in the CDBM model (f). The term f_{E}, which contributes less than 1% to the reduction of transport in the L-mode phase, is not shown in the figure. The position of the ITB foot shown in (d) is the radius where the temperature gradient is maximum, which is also comparable to the radius of a local minimum in the safety factor profile.

The value of $L_{\mathrm{T_e}}^{-1}$ increases with decreasing magnetic shear and saturates when the shear is reversed. A minimum in the value of $f(s, \hat{\alpha})$ is reached approximately at the same time, about 30s for configuration #1 and 50s for configuration #2, which indicate the time of ITB formation for the two configurations, respectively. At these times the total power inside the

electron barrier is about 18MW in the case of configuration #1, which has stronger reverse shear, and just above 20MW in the case of configuration #2, which has positive shear in the core and weaker reverse shear off-axis. The CDBM transport model predicts that the electron barrier forms at lower power in the configuration with stronger reverse shear, consistently with experimental observations in dominant electron heating experiments[1].
Figure 2-(b) compares the total power inside the ion barrier with the threshold power for ITB formation in the ion channel, calculated using Eq.(21) in Ref.[1], inferred from the International ITB database. At the time of ITB formation, the total power inside the ion barrier - which is comparable to the power inside the electron barrier - is above the predicted threshold in both configurations. However, it should be noted that the formula is based on positive shear discharges and has no parameter related to the q-profile, thus the the agreement may be fortuitous.

In configuration #1 the total power inside the barriers decreases after 45s, the transport increases and the magnitude of the electron temperature gradient also decreases, indicating a weakening of the barrier. The EC injected power is stepped up from 13.4 to 20MW at 40s, by adding 6.7MW to the UL, which deposits outside the barrier. In this configuration the ITB foot slowly diffuses inward, as shown in Fig.2d, from the early stages of the barrier formation. On the contrary, the ITB foot is almost constant in configuration #2.

These results indicate that the use of the equatorial launcher is recommended in the early ramp-up phase, for central heating and to form reverse shear profiles in the core that favor the trigger of ITBs.

B. Sustainment of ITBs in the flat-top phase

The previous section covered the ITB formation in L-mode, with central heating between 15s and 75s. At 75s - when the admissible density is reached - the neutral beam injection starts and the L-H transition is set by imposing a pedestal in the density and temperature profile. The neutral beam is gradually stepped-up to full available power (33MW) at 250s.

Figure 1 (right column) shows the profile of EC heating, safety factor, electron and ion temperature, calculated mid-way thru the flattop phase, at 1500s. The current profiles are completely relaxed at this time in both configurations. The safety factor profiles are almost flat in the core, indicating that neither configuration can sustain a moderate reverse shear in

the core in the flattop phase. The current profiles in H-mode are dominated by the neutral beam contribution, which is peaked at about $\rho = 0.3$, as shown in Fig.3. Configuration #1 has a more peaked bootstrap current profile in the core, with a maximum close to the radius where the EL deposits, $\rho_{\rm EL} \simeq 0.35$. This sets the minimum of the safety factor and the ITB foot inside mid-radius. With all the EC power delivered to the upper launcher, the bootstrap current profile is broader, but the neutral beam current still dominates the total current profile. The current driven by the UL is not sufficient to set a minimum in the safety factor off-axis. Without the contribution from the ECCD inside the barrier, a global minimum in q exists inside mid-radius and the temperature profiles are less parabolic than in configuration #1.

The plasma parameters in the relaxed phase are summarized in Table I. The lower current drive efficiency of the upper launcher is compensated by a larger bootstrap current and configuration #2 sustains about 200kA higher non-inductive current than configuration #1, it has 20% higher confinement and 50% higher fusion gain Q. The central temperatures are comparable and close to 15 keV. Both configurations have low normalized $\beta_{\rm N}$ and, even with peaked pressure profiles, the equilibria are ideal MHD stable in the flattop phase. With reference to Fig.17b in Ref.[8], which reports the stability dependence on the pressure peaking factor, these equilibria extrapolate to the ideal MHD stable region at low $\beta_{\rm N}$ and large $p(0)/\langle p\rangle$.

The requested current is 6.5MA in both configurations and the ohmic heating system provides the missing current when the non-inductive current drops below the requested value. The ohmic current contribution, peaked on axis, contributes to the decrease of the safety factor in the core and to the loss of reverse shear, weakening the internal transport barriers. This also causes the current and the vertical forces on the coils to monotonically increase. However, in the case of configuration #1, where the ohmic system has to provide 1.6MA of inductive current, the simulations show that the plasma can get to 3000s without the central solenoid exceeding 10MA and 6T, and the vertical forces exceeding 40MN. These values are below the limits for the central solenoid coils.

For comparison, Table I also shows the plasma parameters obtained for the heating configuration will all the EC power delivered to the upper launcher, but using the modified Coppi-Tang transport model. Here, the ITB foot is evolved in time according to the radius of the minimum safety factor and the parameter C_1 in the thermal diffusivity $[1+C_1(1-\rho/\rho_{\rm b})^2]$

is evolved according to the ratio $C_1 = q(0)/q_{\min}$. The confinement gain is prescribed to be $H_{98} \simeq 1.6$, leading to higher non-inductive current (both from bootstrap and external sources) and higher central temperature. With a prescribed global confinement and with sustained ITBs in the flat-top phase, the values in Table I set a reference for the performance of this scenario, under the hypotheses of this transport model. With pressure peaking factor comparable to those obtained with the CDBM model, the higher normalized beta $\beta_{\rm N} > 2$ calculated with the Coppi-Tang model makes the relaxed equilibrium unstable to the ideal $n = 1$ external kink mode without a wall (but stable with the ITER conforming wall).

IV. STEADY STATE BARRIERS

By trading-off the equatorial and the upper launcher, the day-one heating mix on ITER is capable of triggering ITBs in L-mode and sustaining them in H-mode for a time sufficiently long to avoid coil currents to reach their limit. However, as a consequence of the current profile relaxation and of the contribution from the ohmic current, the magnetic shear flattens in the core and the internal barriers weaken.

In order to find an optimal configuration in the flat-top, *i.e.* one that maximizes the bootstrap current, we have run time-dependent simulations where the deposition radius of the upper launcher and of the equatorial launcher has been scanned within the available range, and we have compared the heating configuration #2 with configurations where one-third of the EC power is delivered to the equatorial launcher also in the flat-top phase. The results of these simulations are summarized in Fig.4, where the bootstrap current and the ECCD in the flattop as a function of the deposition radius are compared.

With all the power delivered to the UL (Fig.4a), the maximum ECCD is measured at $\rho_{\rm UL} \simeq 0.6$; this is not the same position that maximizes the bootstrap current, which is almost constant between 0.6 and 0.7. The maximum in the bootstrap current for $\rho_{\rm UL} \gtrsim 0.70$ will be ignored in the discussion because it occurs at the interface between the region where we use the CDBM model and the Coppi-Tang model, at $\rho \simeq 0.75$.

The upper launcher consists of two steering mirrors (USM and LSM), and the multiple values calculated for the same deposition radius in Fig.4a correspond to cases with variable overlapping between the USM and LSM deposition profiles. It is found that a width of about 1.5 the deposition width from an individual mirror can improve by 3-4% the bootstrap

current compared to having the two mirrors to deposit at the same radius. If the deposition profiles from the individual mirrors are completely separated, the bootstrap current drops, as the cases at $\rho_{\rm UL} \simeq 0.6$ and at $\rho_{\rm UL} \simeq 0.7$ show.

Fig.4b shows the variation of the bootstrap and EC driven current with $\rho_{\rm UL}$ for a configuration where 6.7MW of power are delivered to the equatorial launcher ($\rho_{\rm EL} \simeq 0.37$) and 13.4MW are delivered to the upper launcher (equally shared between the USM and the LSM). A maximum in the bootstrap current is measured at $\rho_{\rm UL} \simeq 0.60$. Contrary to the previous case, both the EC driven current and the bootstrap current decrease outside this radius.

The same current variation, with a maximum for $\rho_{\rm UL} \simeq 0.6$, has been observed when the EL deposition radius is moved between $\rho_{\rm EL} \simeq 0.35$ and $\rho_{\rm EL} \simeq 0.5$. Figure 4c shows the variation of the current with $\rho_{\rm EL}$, for $\rho_{\rm UL} \simeq 0.6$. The total ECCD monotonically decreases with increasing $\rho_{\rm EL}$, while the total bootstrap current is maximum for $\rho_{\rm EL} \simeq 0.45$.

Based on these scans, the launcher configuration with $\rho_{\rm EL} \simeq 0.45$ and $\rho_{\rm UL} \simeq 0.60 - 0.65$ has been used to simulate a new scenario that is shown in Fig.5 and tabulated in the last column of Table I. The equatorial launcher is used in the ramp-up phase to trigger an ITB, then the power delivered to the EL is gradually decreased from 20MW to 6.7MW in the flat-top phase, while the power delivered to the UL is increased. The progressive transition from the equatorial to the upper launcher maintains reverse shear in the core during the ramp-up phase. At the same time the deposition radius of the EL is progressively moved off-axis to $\rho = 0.45$, by increasing the poloidal angle of the bottom launcher (aiming down). As shown in Fig.5c-f, by distributing the EC current over an extended region centered at mid-radius, this configuration maintains a broad bootstrap current profile and a moderate reverse shear until the end of the flat-top phase. The peak in the bootstrap current at $\rho \simeq 0.2$ is a consequence of the ion pressure derivative at this location, which is the dominant contribution to the radial electric field in Eq.2 and causes a localized decrease in the term $f_{\rm E}$.

This configuration sustains 6.2MA of non-inductive current with 53% of bootstrap current, and achieves $Q = 1.62$ with a 30% confinement gain over the H-mode confinement time. Contrary to the other configurations, 15MW of IC power is maintained in the flattop phase to provide central heating and reduce the ohmic contribution.

With a trade-off of the equatorial and upper launcher, the formation and sustainment of

quasi-steady state ITBs could be demonstrated in ITER with the baseline heating configuration. However, with proper constraints from peeling-ballooning theory on the pedestal width and height, the fusion gain and the maximum available non-inductive current are below the target of $Q = 5$ and $I_{\rm P} = 9$MA. Upgrades of the heating and current drive system in ITER, like the use of lower hybrid current drive, which has higher efficiency, could overcome these limitations[8,28].

V. CONCLUSIONS

Extrapolating present day ITB experiments to ITER is challenging because of the limited database available for densities close to the Greenwald limit and for comparable ion and electron temperatures. The dominant ion heating from neutral beam and the presence of a significant toroidal rotation set conditions for ITB formation that are different from those foreseen in ITER, where the $\mathbf{E} \times \mathbf{B}$ flow shear contribution from the toroidal rotation is expected to be low and where the energy confinement times will be longer than the electron-ion thermal equilibration time scales.

ITER steady state scenarios target plasmas with hollow current profiles to maximize the bootstrap current. These plasmas will have magnetic shear profiles reversed in the core. From the limited database available for experiments with dominant electron heating, it is observed that (a) the presence of reverse shear in the core is a necessary condition for formation of ITBs in the electron channel, which (b) typically form at injected powers lowers than the threshold powers for ion transport barriers and (c) ITBs in reversed shear plasmas have their foot locked at the radius of the minimum safety factor[1]. The JT-60U experience indicates that performance can be improved by forming ITBs in the early ramp-up phase with central heating and by heating inside the barrier after their formation[29].

In this work we have applied observations from the available experiments to ITER plasmas and have examined the capability of the baseline heating mix to form and sustain ITBs. Time-dependent simulations with the CDBM transport model show that the central heating from the equatorial launcher is necessary to form ITBs in the ramp-up phase, while the off-axis heating provided by the upper launcher can sustain larger bootstrap current in the flattop phase. With a trade-off of the power distributed between the equatorial and the upper launcher, the formation and sustainment of quasi-steady state ITBs could be thus

demonstrated with the baseline heating and current drive configuration. However, with constrains on the pedestal height, and under the hypotheses of the transport models used, a maximum achievable non-inductive current between 6.2MA and 7.3MA and fusion gain in the range of $Q = 1.6 - 3.4$ are calculated, depending on the transport model used. These values are below the target of 9MA and $Q = 5$. Calculations performed on the same scenarios with different physics-based transport models could reduce the uncertainties in the predictions and improve the confidence interval on the expected regimes of ITER steady state operations.

ACKNOWLEDGMENTS

We thank P. Snyder for providing the EPED1 calculations. S. Ide is kindly acknowledged for fruitful discussion on the early formation of ITBs in JT-60U reverse shear plasmas. This work was supported by the US Department of Energy under contract DE-AC02-CH0911466.

REFERENCES

[1]J. W. Connor, T. Fukuda, X. Garbet, C. Gormezano, V. Mukhovatov, M. Wakatani, the ITB Database Group, and the ITPA Topical Group on Transport and Internal Transport Barrier Physics, Nucl. Fusion **41**, 1823 (2001).

[2]X. Litaudon, Plasma Phys. Control. Fusion **48**, A1–A34 (2006).

[3]G. M. Staebler, Plasma Phys. Control. Fusion **40**, 569 (1998).

[4]R. C. Wolf, Plasma Phys. Control. Fusion **45**, R1–R91 (2003).

[5]M. Wakatani, Plasma Phys. Control. Fusion **40**, 597 (1998).

[6]C. E. Kessel, G. Giruzzi, A. C. C. Sips, R. V. Budny, J. F. Artaud, V. Basiuk, F. Imbeaux, E. Joffrin, M. Schneider, M. Murakami, T. Luce, H. S. John, T. Oikawa, N. Hayashi, T. Takizuka, T. Ozeki, Y.-S. Na, J. M. Park, J. Garcia, and A. A. Tuccillo, Nucl. Fusion **47**, 1274 (2007).

[7]C. E. Kessel, "Development of the iter advanced steady state and hybrid scenarios," (Vienna:IAEA, 2010) `http://www-pub.iaea.org/mtcd/meetings/cn180papers.asp`.

[8]F. M. Poli, C. E. Kessel, M. S. Chance, S. J. Jardin, and J. Manickam, Nucl. Fusion **52**, 063027 (2012).

[9]J. Garcia, G. Giruzzi, J. F. Artaud, V. Basiuk, J. Decker, F. Imbeaux, Y. Peysson, and M. Schneider, Plasma Phys. Control. Fusion **50**, 124032 (2008).

[10]T. J. J. Tala, V. V. Parail, A. Becoulet, G. Corrigan, D. J. Heading, M. J. Mantsinen, P. I. Strand, and contributors to the EFDA-JET Workprogramme, Plasma Phys. Control. Fusion **44**, A495 (2002).

[11]K. Itoh, M. Yagi, S.-I. Itoh, A. Fukuyama, and M. Azumi, Plasma Phys. Control. Fusion **35**, 543 (1993).

[12]A. Fukuyama, K. Itoh, S.-I. Itoh, M. Yagi, and M. Azumi, Plasma Phys. Control. Fusion **37**, 611 (1995).

[13]A. Fukuyama, S. Takatsuka, S.-I. Itoh, M. Yagi, and K. Itoh, Plasma Phys. Control. Fusion **40**, 653 (1998).

[14]S. C. Jardin, J. L. Delucia, and N. Pomphrey, J. Comput. Phys. **66**, 481 (1986).

[15]R. Hawryluk, "An empirical approach to tokamak transport," in *Physics close to thermonuclear conditions*, Vol. 1, edited by B. C. *et al* (Commission of the European Communities, Brussels, 1980) p. 19.

[16]M. Brambilla, "A full wave code for ion cyclotron waves in toroidal plasmas," Rep. IPP 5/66 5/66 (Max-Planck-Institut fur Plasmaphysik, Garching, Computer Science Department, Fanstord, California, 1996).

[17]R. J. Goldston, D. C. McCune, H. H. Towner, S. L. Davis, R. J. Hawryluk, and G. L. Schmidt, J. Comput. Phys. **43**, 61 (1981).

[18]A. Pankin, D. McCune, R. Andre, G. Bateman, and A. Kritz, Comput. Phys. Commun. **159**, 157 (2004).

[19]A. H. Kritz, H. Hsuan, R. C. Goldfinger, and D. B. Batchelor, "Heating in toroidal plasmas," in *Proc. 3rd Joint Varenna-Grenoble Int. Symp., Grenoble*, Vol. 2, edited by CEC (IAEA, Brussels, 1982) p. 707.

[20]M. A. Henderson, R. Chavan, R. Bertizzolo, D. Campbell, J. Duron, F. Dolizy, R. Heidinger, J.-D. Landis, G. Saibene, F. Sanchez, A. Serikov, H. Shidara, and P. Spaeh, Fusion Science and Technology **53**, 139 (2008).

[21]G. Ramponi, D. Farina, M. A. Henderson, E. Poli, G. Saibene, and H. Zohm., Fusion Science and Technology **52**, 193 (2007).

[22]W. M. Tang, Nucl. Fusion **26**, 1605 (1986).

[23]S. C. Jardin, M. G. Bell, and N. Pomphrey, Nucl. Fusion **33**, 371 (1993).

[24]P. B. Snyder, N. Aiba, M. Beurskens, R. J. Groebner, L. D. Horton, A. E. Hubbard, J. W. Hughes, G. Huysmans, Y. Kamada, A. Kirk, C. Konz, A. W. Leonard, J. Lonnroth, C. F. Maggi, R. Maingi, T. H. Osborne, N. Oyama, A. Pankin, S. Saarelma, G. Saibene, J. L. Terry, H. Urano, and H. R. Wilson, Nucl. Fusion **49**, 085035 (2009).

[25]M. Honda and A. Fukuyama, Nucl. Fusion **46**, 580 (2006).

[26]T. S. Hahm and K. H. Burrell, Phys. Plasmas **2**, 1648 (1995).

[27]W. A. Houlberg, Phys. Plasmas **4**, 3230 (1997).

[28]F. M. Poli, C. E. Kessel, and P. T. Bonoli, "Performance and stability of iter steady state scenarios with itbs," (Vienna:IAEA, 2012).

[29]S. Ide and the JT-60U team, J. Plasma Fusion Res. SERIES **4**, 99 (2001).

TABLE I. Plasma parameters calculated at $t = 2500\,\mathrm{s}$. The first column refers to results obtained with the Coppi-Tang model. The other columns refer to results calculated with the CDBM model. Quantities in bold fonts are input to TSC, like the central density $n(0)$ and the requested plasma current waveform I_P.

IC (MW)	20→5	20→5	20→5	20→15
EC (MW) on EL	/	13.4	/	20→6.7
EC (MW) on UL	20	6.7	20	0→13.4
$\mathbf{I_P}$ (MA)	7.3	6.5	6.5	6.5
I_NI (MA)	7.3	4.9	5.1	6.2
I_BS (MA)	4.0	2.3	2.8	3.3
I_NB (MA)	2.9	2.1	2.0	2.4
I_EC (MA)	0.28	0.43	0.25	0.36
P_α	39	9.6	14	22
Q	3.4	0.83	1.2	1.62
n/n_G	0.96	1.0	1.0	1.0
$\mathbf{n(0)[10^{19}m^{-3}]}$	7.0	6.6	6.6	6.5
$T(0)$ (keV)	28	14.4	16.2	22
T_{PED} (keV)	4.0	4.1	4.1	4.1
$p(0)/\langle p\rangle$	3.40	3.35	3.2	3.7
$l_i(1)$	0.97	1.07	0.92	0.97
$q(0)$	2.40	2.01	2.11	2.85
q_{min}	1.78	1.74	1.97	2.02
q_{95}	6.7	7.4	7.4	7.7
β_N	2.24	1.25	1.49	1.77
H_{98}	1.61	1.06	1.2	1.32
$n = 1$, no wall	unstable	stable	stable	stable
$n = 1$, wall	stable	stable	stable	stable

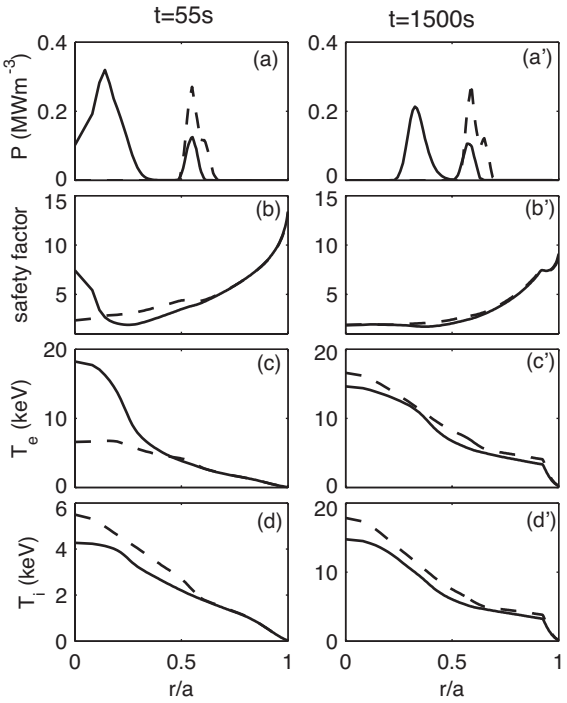

FIG. 1. Profiles calculated at 55s (left) and at 1500s (right) for configuration #1 (solid) and #2 (dash). (a) EC heating deposition (b) safety factor (c) electron temperature (d) ion temperature.

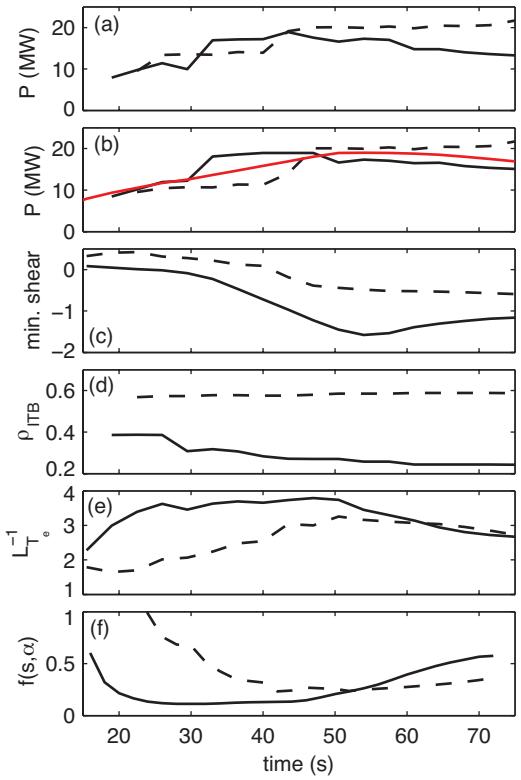

FIG. 2. (Color online) Configuration #1 (solid) and configuration #2 (dashed). (a) total power inside the electron ITB; (b) total power inside the ion ITB, for comparison the theoretical threshold for ion ITB is shown in red. (c) minimum value of the magnetic shear, (d) ITB foot radius, (e) electron temperature inverse gradient scale length (f) contribution from the magnetic shear term in the CDBM model.

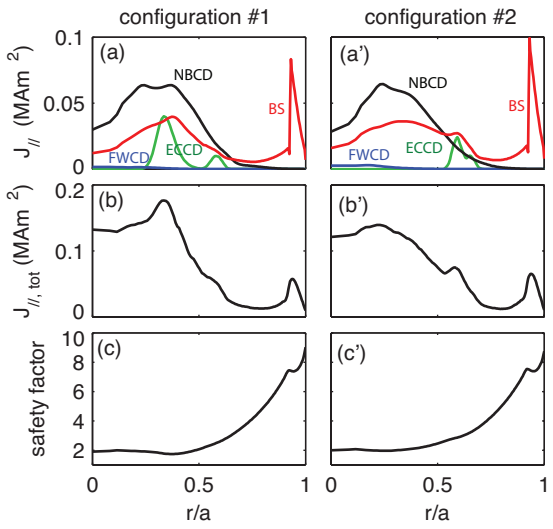

FIG. 3. (Color online) Configuration #1 (left) and configuration #2 (right), profiles calculated at 1500s. (a) toroidal current from the external sources and from the bootstrap mechanism, (b) total toroidal current, (c) safety factor.

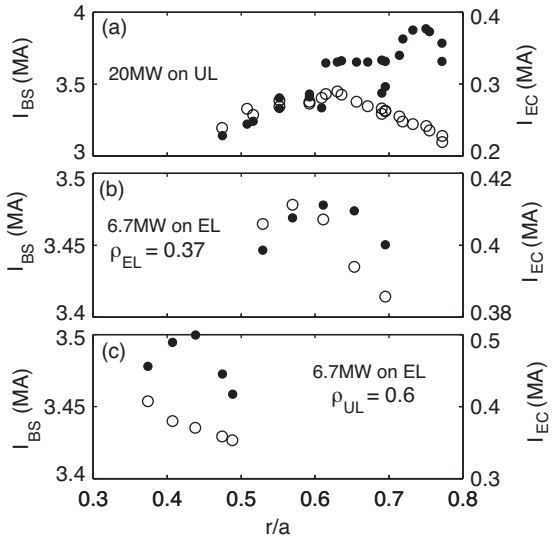

FIG. 4. (a) total bootstrap current (left axis values, solid symbols) and total EC driven current (right axis values, open symbols) variation with the upper launcher deposition radius for a configuration with 20MW of EC power delivered to the upper launcher. (b) bootstrap current and EC driven current for a configuration with 6.7MW of power on the EL (bottom mirror, deposition radius $\rho_{\rm EL} \simeq 0.37$) and 13.4MW on the upper launcher. Variation with respect to the upper launcher deposition radius. (c) bootstrap current and EC driven current for a configuration with 6.7MW on the EL and 13.4MW on the upper launcher. Variation with the EL deposition radius for fixed $\rho_{\rm UL} \simeq 0.61$.

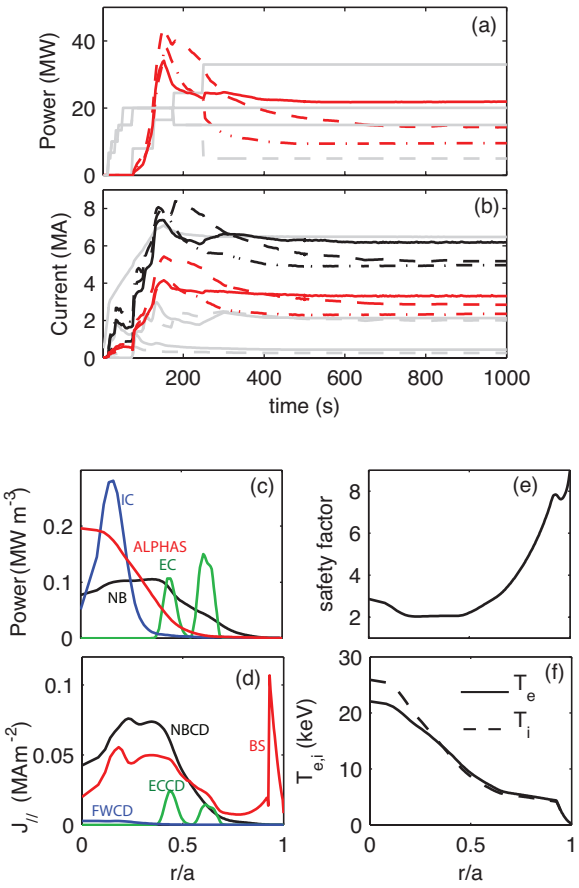

FIG. 5. (Color online) (a) heating and alpha power (b) externally driven and bootstrap current for configuration #1 (dash-dot), configuration #2 (dash) and for a configuration with 6.7MW of EC power on the EL and 13.4MW on the UL (solid). (c) heating profiles, (d) toroidal current profiles , (e) safety factor, (f) electron (solid) and ion (dash) temperature profile for the third configuration, calculated at 2500s.

The Princeton Plasma Physics Laboratory is operated
by Princeton University under contract
with the U.S. Department of Energy.

Information Services
Princeton Plasma Physics Laboratory
P.O. Box 451
Princeton, NJ 08543

Phone: 609-243-2245
Fax: 609-243-2751
e-mail: pppl_info@pppl.gov
Internet Address: http://www.pppl.gov